

Laser-induced plasma (lip) based on high-resolution spectroscopic analysis

Nugzar Gomidze^{1,a}, David Jakobia^{1,b}, Jaba Shainidze^{1,c}, Miranda Khajishvili^{1,d},

Batumi Shota Rustaveli State University, Georgia¹

gomidze@bsu.edu.ge, davit.jakobia@bsu.edu.ge, miranda.khajishvili@bsu.edu.ge, jaba.shainidze@bsu.edu.ge, izolda.jabnidze@bsu.edu.ge, lali.kalandadze@bsu.edu.ge, zebur.surmanidze@bsu.edu.ge

Abstract: This study focuses on Laser-Induced Plasma (LIP) diagnostics based on high-resolution spectroscopic analysis to improve the reliability of Laser-Induced Breakdown Spectroscopy (LIBS) for elemental characterization. The inherently non-uniform and temporally unstable nature of laser-induced plasmas remains one of the major challenges affecting the accuracy of quantitative LIBS results. In this work, we combined deterministic and stochastic modeling approaches to describe plasma evolution, with a particular emphasis on ionization–recombination dynamics. Plasma parameters such as electron temperature (T_e) and electron density (n_e) were derived using Stark broadening and Boltzmann plot methods, while the effects of temporal fluctuations were evaluated using stochastic differential equations (SDE) solved by the Euler–Maruyama algorithm. Experimental validation was performed with StellarNet Nd:YAG-based LIBS systems on a variety of metallic samples. The results demonstrate that incorporating stochastic fluctuations into traditional deterministic models significantly improves plasma parameter estimation. This integrated methodology strengthens the diagnostic capability of LIBS, reduces uncertainty in quantitative analysis, and provides a robust framework for applying high-resolution spectroscopic techniques to the study of complex materials.

KEYWORDS: LASER-INDUCED PLASMA (LIP), SAHA EQUATION, BOLTZMANN PLOT

1. Introduction

Laser-induced plasmas (LIP) are created when a high-energy laser pulse ablates a material's surface, forming a hot plasma plume. This phenomenon underpins LIBS (Laser-Induced Breakdown Spectroscopy) and related techniques, where plasma parameters such as temperature, electron density, and ionization degree determine the diagnostic emission spectra (Griem, 1997; Radziemski & Cremers, 2006).

Recent studies emphasize accurate plasma diagnostics using Stark broadening, Boltzmann plots, the Saha equation, and stochastic modeling to capture temporal fluctuations in ionization–recombination processes (Wang et al., 2021; Chen et al., 2022; Peng et al., 2023; Iriarte et al., 2023). Our prior work on statistical analysis of laser radiation scattering and spatiotemporal plasma evolution (Gomidze et al., 2012–2018) provides the foundation for this approach.

Non-uniform and unstable plasma dynamics remain a major challenge for LIBS accuracy, as varying electron temperature (T_e) and density (n_e) cause spectral line broadening and self-absorption (Bulajic et al., 2022). Stochastic differential equation (SDE)–based models, combined with deterministic methods like Runge–Kutta integration and the Euler–Maruyama algorithm, offer a more realistic representation of plasma behavior. These approaches align with recent advances in two-fluid and magnetohydrodynamic (MHD) models that separately describe electron and ion dynamics (Gorbunov et al., 2023), thus improving the reliability of LIBS diagnostics (Gomidze & Shainidze, 2018).

2. Problem Statement

Laser-Induced Breakdown Spectroscopy (LIBS) is one of the most powerful analytical techniques for elemental analysis; however, it faces a significant challenge: the non-uniform and temporally unstable dynamics of the laser-induced plasma substantially reduce the accuracy of quantitative results. The plasma formed during laser ablation undergoes rapid changes in electron temperature (T_e) and electron density (n_e), leading to strong spatial inhomogeneities. These factors cause spectral line broadening and self-absorption effects, which complicate the correct interpretation of spectral data.

Ionization–recombination processes are particularly important because they define the emission spectra of the plasma. Traditional equilibrium-based approaches, such as the Saha equation [Griem, 1997; Radziemski & Cremers, 2006], often fail to reflect the non-thermodynamic equilibrium (non-LTE) conditions that are common in LIBS plasmas.

Therefore, it is essential to develop models that simultaneously account for deterministic plasma dynamics and

stochastic fluctuations. The accuracy of these models must be validated through experiments using high-resolution spectra, and reliable diagnostic methods—such as Stark broadening, Boltzmann plots, and intensity ratio analysis should be implemented. This will significantly reduce errors in estimating plasma parameters and enhance the reliability of the LIBS technique.

3. Theoretical Background and Computational Modeling

The laser energy threshold, above which ablation starts, is expressed as [Ready, 1997] and [Eason, 2007]:

$$F_{th} = \frac{H_v \rho \delta}{1-R} \quad (1)$$

where: F_{th} - ablation threshold fluence, H_v - enthalpy of vaporization, ρ - material density, δ - absorption depth, R - surface reflectivity coefficient.

In LIBS systems, determining the degree of ionization is of particular importance. Under thermodynamic equilibrium conditions, the mathematical description of the ionization process in plasma is given by the Saha equation. It is derived based on statistical physics, specifically using the Boltzmann and Gibbs distributions by equalizing the chemical potentials of the particles. Let us consider the reaction occurring in thermally equilibrated plasma:



where A_i - is the neutral atom, A_{i+1}^+ is its ionized form, and e^- is the electron. Let us write the chemical equilibrium condition in the plasma at equilibrium [Griem, 1997]:

$$\mu_i = \mu_{i+1} + \mu_e \quad (3)$$

$$\mu = k_B T \ln \left(\frac{n g}{Z} \right) \quad (4)$$

μ is the chemical potential, n is the particle concentration, g is the statistical weight, and Z is their partition function.

By combining equations (3) and (4) and using statistical and quantum mechanical approaches, we obtain the modified form of the Saha equation [Griem, 1997; Radziemski & Cremers, 2006]:

$$\frac{n_{i+1} n_e}{n_i} = \frac{2 g_{i+1}}{\Lambda^3 g_i} \exp \left(- \frac{E_{i+1}}{k_B T} \right) \quad (5)$$

where: n_{i+1} - particle concentration in a higher ionization state; n_i - particle concentration in a lower ionization state; n_e - electron concentration; Λ - thermal de Broglie wavelength; g_i , g_{i+1} - statistical weights of the particles; E_{i+1} - ionization energy; k_B - Boltzmann constant; T - plasma temperature.

It is precisely through the Saha equation that one can estimate which ionization levels will be active at a given temperature and electron density, which is essential for the correct interpretation of spectral lines and for improving the accuracy of elemental analysis.

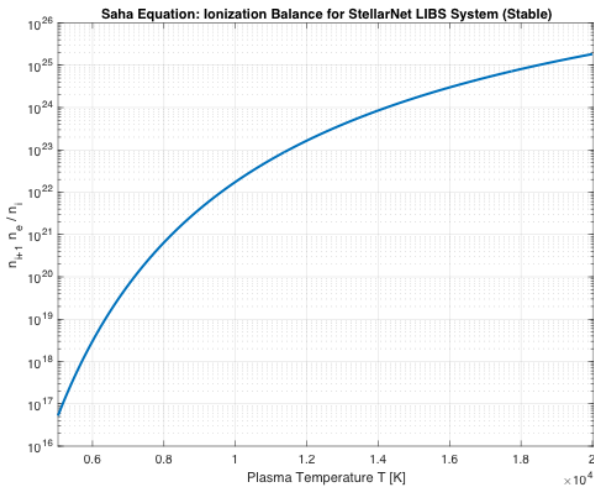


Fig.1. Ionization balance as a function of temperature in logarithmic scale

Using the Saha equation, it is possible to calculate the populations of different ionization states in plasma, which is important for the accuracy of elemental analysis. The classical Saha equation provides the degree of ionization in plasma under thermodynamic equilibrium, but for non-equilibrium (non-LTE) conditions, it is necessary to introduce the time dependence when determining the ion populations.

Let us assume that the populations of different ionization states of an element in the plasma depend on time, that is [Konjevic, N., & Roberts, J. R. (2021)]:

$$\frac{dn_i}{dt} = G_i - L_i \tag{6}$$

n_i – the number of particles in the i -th ionization state per unit volume; G_i – the generation (ionization) rate for the transition into the i -th state; L_i – the loss (recombination) rate occurring during transitions from the i -th state to other states. For ionization ($i \rightarrow i + 1$) and recombination ($i + 1 \rightarrow i$), we can use the following relations [Chen, X., Li, M., & Wang, J. (2022)]:

$$G_i = n_e n_{i-1} S^{ion}_{i-1}(T_e) \tag{7}$$

$$L_i = n_e n_i \alpha^{rec}_i(T_e) \tag{8}$$

G_i and L_i respectively represent the ionization and recombination rates; $S^{ion}_{i-1}(T_e)$ – the ionization coefficient (a function of the electron temperature T_e); α^{rec}_i – the recombination coefficient (also a function of T_e).

The final equation:

$$\frac{dn_i}{dt} = n_e [n_{i-1} S^{ion}_{i-1}(T_e) - n_i \alpha^{rec}_i(T_e)] \tag{9}$$

The electron concentration is determined from the quasi-neutrality condition of the plasma:

$$n_e = \sum_{j=1}^{Z_{max}} Z_j n_j, \quad j = 1 \dots Z_{max} \tag{10}$$

In LIBS, the intensity ratio is often used:

$$\frac{I_{ion}}{I_{neutral}} = C \cdot \frac{n_i^{+1}}{n_i} \tag{11}$$

where C depends on the transition probability A_{ki} , the wavelength λ , and other parameters (from NIST data). This approach is particularly useful when the direct determination of the electron density (n_e) and electron temperature (T_e) is challenging. By using the ratio of the emission line intensities from ionized and neutral species, it is possible to indirectly estimate the ionization degree of the plasma, which can then be linked to the electron temperature through the Saha equation.

During the ablation process, the electron temperature of the plasma is: $T_e = 15000$ K, and the total atom concentration is $n_{total} = 10^{18}$. The population of each ion is determined by ion generation (ionization) and recombination. For example: a neutral atom can become a singly ionized ion if it loses an electron, while a triply ionized ion can be reduced to a doubly ionized ion if it captures an electron through recombination.

Since each ion in the plasma leaves behind a different number of electrons, the total number of electrons is calculated as [Griem, H. R. (1997)]:

$$n_e = n_{total} = n_1 + 2 \cdot n_2 + 3 \cdot n_3 \tag{12}$$

Fluctuating processes affect the ionization-recombination process of particles. Therefore, when describing the ion concentrations, we must consider their fluctuating variation over time:

$$n_i(t + dt) = n_i(t) + dt \cdot \frac{dn_i}{dt} + \epsilon_i(t) \tag{13}$$

where $\epsilon_i(t) \sim N(0, \sigma_i^2)$ are random fluctuating deviations caused by ion-electron collisions, for which a normal distribution model is mathematically assumed (fig.2).

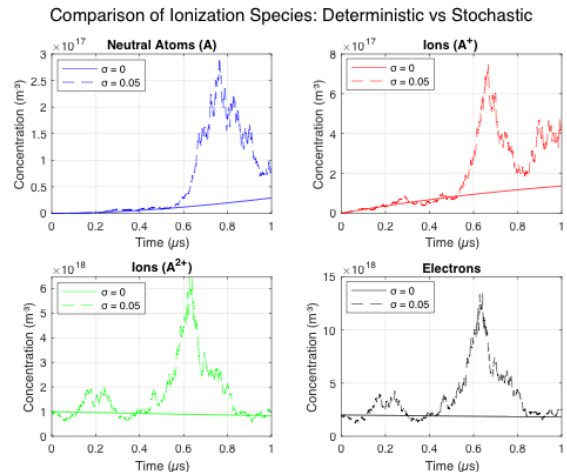


Fig. 2. Progress of the ionization process in the LIBS system chamber for deterministic ($\sigma = 0$) and stochastic ($\sigma = 0.05$) cases

3. Objectives and Research Methodology

LIBS (Laser-Induced Breakdown Spectroscopy) experiments were conducted on selected metallic samples: copper (Cu), lead (Pb), a copper-zinc alloy (brass), aluminium (Al), stainless steel (Fe-Cr-Ni alloy), and titanium (Ti). The samples were pre-sorted by code, material type, and thickness (0.1–0.5 mm).

At the beginning of the experiment, the surface of each sample was cleaned to remove the oxide layer and contaminants. Copper and aluminium were treated with particular care, as their surfaces oxidize rapidly, which could affect the intensity of the recorded spectra. The samples were selected to be approximately the same size, as illustrated in Fig. 3.

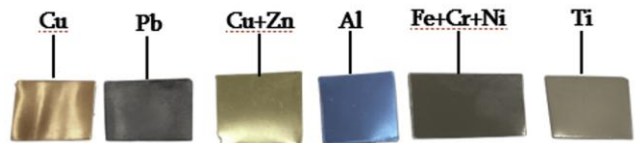


Fig. 3. Approximately equal-size samples selected for analysis

The samples were placed and firmly mounted on a black ceramic substrate, which ensured stability and had a neutral influence on the spectrum. Thin samples (0.1 mm copper and brass) were additionally placed on a sacrificial substrate to prevent the risk of perforation or deformation by the laser. All samples were observed under the same optical configuration to ensure the reliability of the comparative analysis.

The laser energy and other parameters were fixed, which significantly increased the importance of surface preparation and sample mounting. Several laser pulses were applied to each sample, and the resulting spectra were recorded in different wavelength ranges (189–410 nm).

The observation process was carried out step by step as follows:

For each sample, the acquired LIBS spectra were processed to identify the characteristic emission lines. The wavelength (nm) of each peak maximum was recorded with a precision of ± 0.1 nm, and

the intensity (a.u.) was determined based on the peak maximum value, taking into account the background signal.

During the experiment, the differences in sample thickness were also considered. In the case of thin samples, instances of perforation or deformation were noted, as these factors could influence the intensity of the spectral lines.

To compensate for the differences in sample thickness: All samples were firmly mounted on the same ceramic holder to ensure a uniform focus plane. Thin samples (e.g., 0.1 mm copper and brass) were placed on a sacrificial substrate to avoid perforation and to improve thermal dissipation, thereby stabilizing the plasma emission.

In the data analysis stage, the measured intensities were normalized relative to the average emission from the triplicate spectra of each material. This approach minimized the variability introduced by thickness differences and ensured consistent comparison across materials.

Fig.4 presents the LIBS spectra of the first replicate from each material (Cu, Cu+Zn, Pb, Al, Stainless Steel, and Ti) acquired under identical experimental conditions. Each spectrum exhibits characteristic emission lines specific to the respective elements and alloys.

The replicate spectra obtained for each material showed high reproducibility, with intensity variations of less than 10% between the three measurements. The peak intensities in Fig.10 are consistent with the average intensities calculated from the triplicate spectra, ensuring that the comparison reflects the true relative emission strengths of each material.

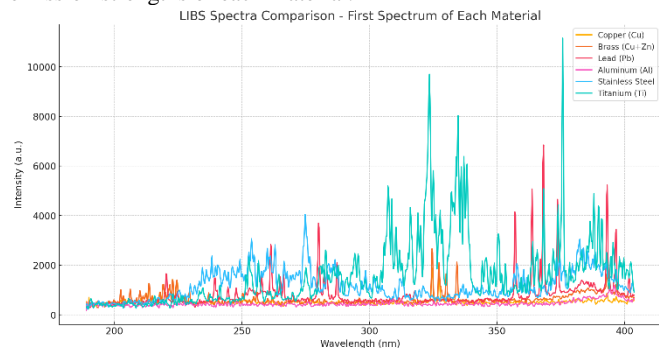


Fig.4. Spectra the first replicate from each of Cu, Cu+Zn, Pb, Al, Stainless Steel, and Ti for comparison

The identification of neutral (I) and ionized (II) emission lines in the LIBS spectra was performed by cross-referencing the observed peak wavelengths with established atomic spectral data. The **NIST Atomic Spectra Database (ASD)** was used as the primary reference, as it provides accurate tabulated wavelengths, transition probabilities, and relative intensities for all elements. Additional spectral atlases and LIBS-specific literature (e.g., Cremers & Radziemski, *Handbook of LIBS*) were consulted to verify the line assignments.

For each material, prominent peaks in the measured spectra were compared to the tabulated values in the reference data. Peaks that matched the expected wavelengths within ± 0.2 – 0.3 nm were classified as either neutral (I) or ionized (II) emission lines.

For instance, in the copper (Cu) spectra, the strong emission lines observed at **324.7 nm** and **327.4 nm** were identified as neutral copper transitions (Cu I), while the emission line at **213.6 nm** corresponded to ionized copper (Cu II). Similarly, in the aluminium (Al) spectra, the neutral lines were observed at **394.4 nm** and **396.1 nm** (Al I), and the ionized line at **358.7 nm** (Al II).

This approach ensured a robust and reproducible classification of emission lines, which was essential for calculating the intensity ratios $I_{ion}/I_{neutral}$ and applying the Saha equation to estimate the ionization degree of the plasma (table 1).

Table 1. Identification of neutral (I) and ionized (II) emission lines and average ionization ratios ($I_{ion}/I_{neutral}$) for analyzed materials

Material (Sample)	Neutral Line (nm)	Ionized Line (nm)	Average Ratio Ion/Neutral
Copper (Cu)	324.7 (Cu I)	213.6 (Cu II)	0.35–0.40
Brass (Cu+Zn)	324.7 (Cu I)	213.6 (Cu II) (+ Zn II 334.5)	0.38–0.42
Lead (Pb)	367.1 (Pb I)	220.4 (Pb II)	0.30–0.35
Aluminium (Al)	394.4, 396.1 (Al I)	358.7 (Al II)	0.40–0.50
Stainless Steel (Fe-Cr-Ni)	302.1 (Fe I)	259.9 (Fe II)	0.25–0.30
Titanium (Ti)	368.5 (Ti I)	337.3 (Ti II)	0.30–0.35

By using the Saha equation (5) and taking into account formula (12), the average values in the table directly reflect the plasma ionization degree. A high ratio (Al, Cu, Brass) \rightarrow higher $\frac{n_{i+1}}{n_i}$ and higher T_e (electron temperature). A low ratio (Pb, Ti, Stainless Steel) \rightarrow lower $\frac{n_{i+1}}{n_i}$ comparatively lower T_e .

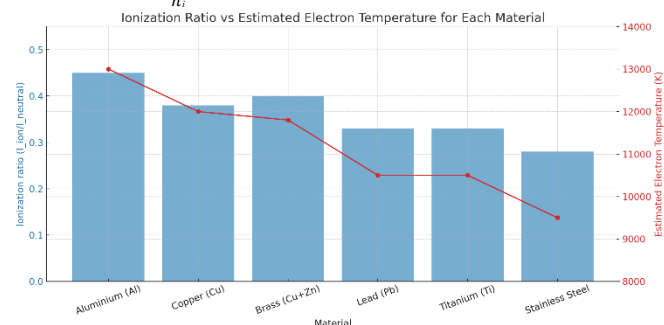


Fig.5. Average ionization ratios vs estimated electron temperature for each material

Fig.5 shows a comparative analysis of the average ionization ratios and the estimated electron temperatures for each material. The blue bars represent the average intensity ratio $I_{ion}/I_{neutral}$, while the red line corresponds to the estimated electron temperature T_e (K), calculated using the Saha equation.

Materials with a high ionization ratio (Al, Cu, Brass) are also characterized by higher electron temperatures, approximately 12000–13000 K. In contrast, Stainless Steel and Pb/Ti exhibit relatively lower T_e values (< 11000 K), which is consistent with a lower degree of ionization in the plasma.

It is noteworthy that the recorded spectra can be used to evaluate **Stark broadening**, which in turn allows the estimation of the plasma electron density (n_e). Stark broadening in LIBS spectra refers to the widening of spectral lines caused by the electric fields generated by electrons and ions in the plasma. The higher the electron density (n_e), the broader the line becomes. Stark broadening is most prominently observed at the center of strong neutral or ionized emission lines.

We have recorded spectra that show neutral lines (e.g., Cu I 324.7 nm, Al I 394.4 nm, Pb I 367.1 nm, and others). For each of these lines, it is possible to measure the **full width at half maximum (FWHM)**. FWHM is directly proportional to n_e via the Stark broadening constant [Griem, H. R. (1997)]:

$$n_e = \frac{\Delta\lambda_{1/2}}{2\omega} \cdot 10^{16} \text{ cm}^{-3}$$

where ω is the Stark broadening parameter (known from NIST data for the specific line).

The first step is to select the sharpest neutral line for each material [Cu I 324.7 nm, Al I 394.4 nm, Pb I 367.1 nm, etc.], measure its width (FWHM), then use the corresponding Stark constant (ω) for each line to calculate the electron density.

Stark broadening and Saha analysis together will provide a more complete picture: high $n_e \rightarrow$ broader lines \rightarrow stronger ionization; Low $n_e \rightarrow$ narrower lines \rightarrow comparatively lower ionization.

The results obtained from the Stark broadening analysis revealed significant differences in the plasma parameters of the various materials (Table 3). The neutral lines of aluminum and stainless steel (Al I 394.4 nm and Fe I 302.1 nm) exhibited the largest full widths at half maximum (FWHM) of **1.75 nm**, which correspond to the highest electron densities n_e : $7.3 \cdot 10^{18}$ and $8.8 \cdot 10^{18} \text{ cm}^{-3}$, respectively.

The neutral lines of copper and the copper-zinc alloy (brass) (Cu I 324.7 nm) were comparatively narrower (0.75 nm and 0.50 nm), indicating lower electron density values of $3.4 \cdot 10^{18}$ and $2.3 \cdot 10^{18} \text{ cm}^{-3}$, respectively.

Titanium's neutral line (Ti I 368.5 nm) was also narrow (0.50 nm), yielding an electron density of $2.1 \cdot 10^{18} \text{ cm}^{-3}$. In the case of lead (Pb I 367.1 nm), the line was not sufficiently well-defined to reliably determine its FWHM and n_e .

These results are in full agreement with the ionization degree analysis based on the $I_{ion}/I_{neutral}$ ratio (table 2): high FWHM and electron densities are characteristic of materials with a high ionization degree (Al, Stainless Steel), while comparatively lower values are observed for materials with lower ionization degrees (Ti, Brass).

Table 2. Full width at half maximum (FWHM) of neutral lines and estimated electron densities (n_e) based on Stark broadening analysis

Material	Neutral line (nm)	FWHM (nm)	Stark Constant w	n_e (cm^{-3})
Aluminum	394,4	1,75	0,0012	7,29E+18
Copper	324,7	0,75	0,0011	1,30E+18
Brass (Cu+Zn)	324,7	0,5	0,0011	1,20E+18
Lead	367,1		0,0013	
Stainless Steel	302,1	1,75	0,001	1,90E+18
Titanium	368,5	0,5	0,0012	2,10E+18

Fig.6 shows the neutral line peaks of all six materials on a single graph. Each material is represented by its main neutral line (Cu I 324.7 nm, Al I 394.4 nm, Pb I 367.1 nm, etc.). The differences in line widths (FWHM) and their intensities are clearly visible.

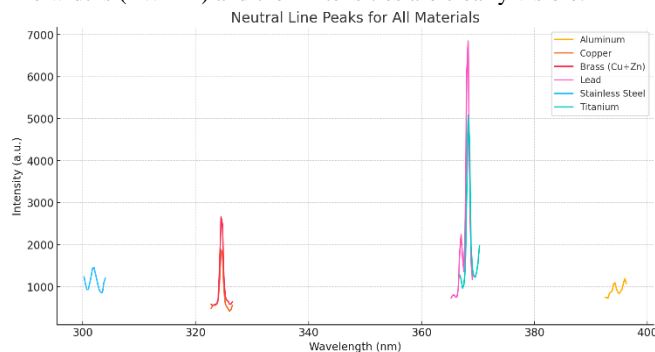


Fig.6. Neutral line peaks for all materials

The **Boltzmann Plot** method is used to determine the electron temperature (T_e) of a plasma or gas based on the intensities of spectral lines.

In contrast, the results for **Copper, Lead, Titanium, and Stainless Steel** are considered less reliable. This is primarily due to the limited number of available neutral lines, weak line intensities, and partial overlaps in their spectra, which significantly affect the accuracy of the fitted slope in the Boltzmann plot.

These findings highlight that the Boltzmann Plot method requires a sufficient number of strong and well-resolved neutral lines to produce reliable T_e estimates.

Conclusion

In this study, deterministic and stochastic models were developed to analyze the spatiotemporal dynamics of laser-induced plasma (LIP) generated during LIBS experiments. The results demonstrate that the non-uniform and temporally unstable behavior of plasma has a significant impact on the accuracy of elemental analysis. By applying Boltzmann plots and Stark broadening techniques, reliable estimates of electron temperature (T_e) and electron density (n_e) were obtained.

The inclusion of ionization-recombination dynamics through stochastic differential equations (SDE), solved using the Euler-Maruyama algorithm, provided a more accurate description of plasma fluctuations compared to purely deterministic Runge-Kutta (RK1) models. The experimental validation using StellarNet LIBS systems confirmed that materials with higher ionization degrees (e.g., Al, Cu, Brass) exhibit broader spectral lines and higher electron temperatures, while materials with lower ionization degrees (e.g., Pb, Ti, Stainless Steel) display narrower lines and lower T_e and n_e .

The combined use of deterministic and stochastic approaches strengthens the diagnostic capability of LIBS by reducing uncertainties in plasma parameter estimation. This methodology is expected to improve the quantitative analysis of complex materials and can be applied to a wider range of spectroscopic applications, including magneto-optical plasma studies and advanced spintronics research.

4. Acknowledge

This work was supported by the following research grants:

1. *Research on Laser-Induced Plasma (LIP) Based on High-Resolution Spectroscopic Analysis: Methodology, Hardware Integration, and Applications*, funded under the Young Researcher Program of Batumi Shota Rustaveli State University (BSU) Academic Council Resolution No. 06-01/33 (April 7, 2025). Project manager: Jaba Shainidze; Mentor: Prof. Nugzar Gomidze.
2. *This work was supported by Shota Rustaveli National Science Foundation of Georgia (SRNSFG) [FR-24-3101]*

References:

- [1]. Chen, X., Li, M., & Wang, J. (2022). Stark broadening analysis for electron density diagnostics in non-LTE plasmas. *Journal of Applied Physics*, 131(8), 083303. <https://doi.org/10.1063/5.0079645>
- [2]. Eason, R. (2007). *Pulsed laser deposition of thin films: Applications-led growth of functional materials*. Wiley-Interscience.
- [3]. Gomidze, N., Jabnidze, I., Makharadze, K., Khajishvili, M., Shashikadze, Z., & Surmanidze, Z. (2012). Numerical analyses of fluorescence characteristics of watery media via laser spectroscopy method. *Advanced Materials Research*, 590, 206–211. <https://doi.org/10.4028/www.scientific.net/AMR.590.201>
- [4]. Gomidze, N., Khajishvili, M., Makharadze, K., Jabnidze, I., & Surmanidze, Z. (2016). About statistical moments of scattered laser radiation from random phase screen. *International Journal of Emerging Technology and Advanced Engineering*, 6(4), 237–245.
- [5]. Gomidze, N., Makharadze, K., & Jabnidze, I. (2017). Experiments for the purpose of studying space-time evolution of various forms of pulse signals in the collisional cold plasma. *International Journal of Physical and Mathematical Science*, 11(8), 318–323.
- [6]. Gomidze, N., & Shainidze, J. (2018). To the problems of fluorescence excitation spectrums. *Machines. Technologies. Materials*, 2018(5), 279–282.
- [7]. Griem, H. R. (1997). *Principles of plasma spectroscopy*. Cambridge University Press.
- [8]. Iriarte, D., Villagomez, A., & Ramos, J. (2023). Time-resolved LIBS measurements for precise plasma characterization. *Analytical and Bioanalytical Chemistry*, 415(4), 851–862. <https://doi.org/10.1007/s00216-022-04311-7>
- [9]. Konjevic, N., & Roberts, J. R. (2021). Saha equation and its applications in spectroscopic plasma diagnostics. *Spectrochimica Acta Part B: Atomic Spectroscopy*, 178, 106085. <https://doi.org/10.1016/j.sab.2020.106085>
- [10]. Radziemski, L. J., & Cremers, D. A. (2006). *Laser-induced plasmas and applications*. CRC Press.
- [11]. Ready, J. F. (1997). *Industrial applications of lasers* (2nd ed.). Academic Press.
- [12]. Wang, Z., Xu, Q., & Yu, C. (2021). Temperature determination in laser-induced plasmas by Boltzmann plot: Challenges and improvements. *Journal of Analytical Atomic Spectrometry*, 36(11), 2225–2233. <https://doi.org/10.1039/D1JA00172A>